Biophysical Journal
Article

Biophysical Society

Molecular mechanisms of spontaneous curvature and softening in complex lipid bilayer mixtures

Henry J. Lessen,[1] Kayla C. Sapp,[1] Andrew H. Beaven,[1,2] Rana Ashkar,[3,4] and Alexander J. Sodt[1,*]
[1]Eunice Kennedy Shriver National Institute of Child Health and Human Development, National Institutes of Health, Bethesda, Maryland; [2]Postdoctoral Research Associate Program, National Institute of General Medical Sciences, National Institutes of Health, Bethesda, Maryland; [3]Department of Physics, Virginia Tech, Blacksburg, Virginia; and [4]Center for Soft Matter and Biological Physics, Virginia Tech, Blacksburg, Virginia

ABSTRACT Membrane reshaping is an essential biological process. The chemical composition of lipid membranes determines their mechanical properties and thus the energetics of their shape. Hundreds of distinct lipid species make up native bilayers, and this diversity complicates efforts to uncover what compositional factors drive membrane stability in cells. Simplifying assumptions, therefore, are used to generate quantitative predictions of bilayer dynamics based on lipid composition. One assumption commonly used is that "per lipid" mechanical properties are both additive and constant—that they are an intrinsic property of lipids independent of the surrounding composition. Related to this is the assumption that lipid bulkiness, or "shape," determines its curvature preference, independently of context. In this study, all-atom molecular dynamics simulations on three separate multilipid systems were used to explicitly test these assumptions, applying methodology recently developed to isolate properties of single lipids or nanometer-scale patches of lipids. The curvature preference experienced by populations of lipid conformations were inferred from their redistribution on a dynamically fluctuating bilayer. Representative populations were extracted by both structural similarity and semi-automated hidden Markov model analysis. The curvature preferences of lipid dimers were then determined and compared with an additive model that combines the monomer curvature preference of both the individual lipids. In all three systems, we identified conformational subpopulations of lipid dimers that showed non-additive curvature preference, in each case mediated by a special chemical interaction (e.g., hydrogen bonding). Our study highlights the importance of specific chemical interactions between lipids in multicomponent bilayers and the impact of interactions on bilayer stiffness. We identify two mechanisms of bilayer softening: diffusional softening, driven by the dynamic coupling between lipid distributions and membrane undulations, and conformational softening, driven by the inter-conversion between distinct dimeric conformations.

SIGNIFICANCE Cells must expend energy to deform and reshape membranes for necessary biological functions. The work required to accomplish these tasks is directly dependent on the molecular composition of the target membranes. Additionally, many biologically important lipids form multimeric complexes within the bilayer. Knowing how inter-molecular association alters the curvature preference of lipids is crucial to understanding the impact of complex biological lipid composition on the shapes of lipidic structures in cells.

INTRODUCTION

Compositional heterogeneity in cellular membranes is necessary for function (1). The bilayer and its constituent lipids are important for many essential functions including signaling (2–4), chemical separation (5), intracellular sorting (6), metabolism (7), and biogenesis (8). In eukaryotic cells, different organelles have well-defined lipid compositions (1), and deviations from normal lipid composition indicate stress or pathology. Membranes also show compositional asymmetry in their leaflets (9), enriching the possibilities for functional roles of lipid composition. Finally, bilayers are not well mixed within the leaflet and frequently display enrichment of particular lipid types in specific regions and shapes (10,11). For example, lipid-dependent spatial correlations of surface receptors directly tie compositional affinity to cellular signaling processes (12). Stresses due to lipid chemistry (i.e., deviation from preferred geometry) not only influence local mechanics but also protein function (13–15). Because of the extensive physiological role and great chemical diversity of lipids in the cell, it is

Submitted February 25, 2022, and accepted for publication July 28, 2022.
*Correspondence: alexander.sodt@nih.gov
Henry J. Lessen and Kayla C. Sapp contributed equally to this work.
Editor: Michael F. Brown.
https://doi.org/10.1016/j.bpj.2022.07.036

imperative to understand how the energetics of native bilayers depend on its many components.

More work is required to relate findings from model membranes (typically one to three lipid species) to biological membranes (hundreds of lipid species). It is often assumed that membrane properties are directly proportional to relative amounts of different lipids, but this is not always the case. For example, cell-extracted giant plasma membrane vesicles have lower bending moduli (κ_b) than their model counterparts. The bending modulus of cell-extracted giant plasma membrane vesicles was measured to be ~20 k_BT (16). This is considerably lower than giant vesicles of fluid membranes like 1,2-dioleoyl-sn-glycero-3-phosphocholine (DOPC) (26 k_BT (17)) and a liquid-disordered phase mixture of DOPC, cholesterol, and sphingomyelin (46 k_BT (18)). Similar observations have been seen when comparing the area compressibility modulus of red blood cell extract to model membrane mixture representative of the major lipid types (19). The bending stiffness is of fundamental interest to membrane remodeling events, as it controls the overall energetic scale. The mechanism behind κ_b reduction is important for understanding the forces that drive many cellular processes.

To address the discrepancies between biological systems and their simplified models, it is necessary to understand how lipid mixtures differ from homogeneous bilayers. Leibler has previously described how bilayers will soften as a result of the dynamic redistribution of curvature-sensitive inclusions (20). In the supporting material, we derive (using the Helfrich/Canham model modified for local lipid energetics (21)) the softening factor α yielding the apparent bending modulus $\kappa_{app.}$ in our own notation:

$$\kappa_{app.} \approx [1 - \alpha(\Delta c_0, \chi)]\kappa_b \tag{1}$$

$$\alpha(\Delta c_0, \chi) = \frac{A_p(\Delta c_0)^2 \kappa_b \chi(1 - \chi)}{2k_BT}, \tag{2}$$

where Δc_0 is the difference of spontaneous curvature of the inclusion compared with the bulk, χ is the inclusion mole fraction, κ_b is the bilayer bending modulus, and A_p is the area of the inclusion. Consider, for example, a mixture of PE and PC lipids, with $\Delta c_0 \approx 0.02$ Å^{-1}, $A_p \approx 65$ Å^2, $\chi = 0.5$, and $\kappa_b \approx 14$ kcal/mol, yields an 8% reduction in the bending modulus. For additional discussion of softening in lipid bilayers with mixed composition, refer to refs. (22–25).

The correct identification of both the temporal and spatial scale driving softening is necessary for identifying the softening mechanism. As such, we have defined two possible mechanisms of softening that rely on differences in the spontaneous curvature of lipids: diffusional and conformational. Our proposed mechanisms differ in two major ways: origin of Δc_0, and timescale of redistribution. Diffusional softening is caused by the lateral distribution of lipids with different curvature preferences to membrane undulations. The timescale for this softening depends on both the timescales of lipid diffusion and the membrane undulations (21). For example, a bilayer composed of minor species lipid A (l_A) (non-zero curvature) and matrix lipid B (l_B) (zero curvature) would exhibit this softening. Alternatively, conformational softening is due to the dynamic inter-conversion between curvature sensitive lipid conformations. This mechanism depends on the timescale governing inter-conversion between these curvature sensitive states. Importantly, knowledge of curvature-dependent lipid conformations is needed for this mechanism and is at odds with some common assumptions used in continuum membrane models. Both mechanisms result in softening described by Eq. 2.

Continuum models, like the Helfrich/Canham formalism (26,27), use simplifying assumptions to calculate the energetics of membrane deformations. One such assumption is that per-lipid continuum properties (i.e., spontaneous curvature, bending modulus, and area compressibility) are additive, i.e., the properties of the whole system are the linear sum of its parts. Employing the additive assumption dramatically reduces the complexity of heterogeneous membrane energetics, and indeed the assumption is supported experimentally in many cases. For example, the spontaneous curvature of cholesterol is similar in both PE and PC matrices (28). This is, however, not always the case. Experiments on hexagonal phases indicate non-additive curvature preferences of palmitoyl sphingomyelin (PSM) mixtures with certain ceramides (29). In cholesterol-rich bilayers, simulations indicate curvature energetics vary non-linearly with tail saturation (30). Additionally, the formation of specific molecular interactions (in this case, hydrogen bonds) leads to a non-linear relationship between lipid content and curvature preference (30). These exceptions highlight the importance of understanding how complex formation between lipid components alters the additive assumption for the continuum description of the bilayer. Current molecular simulation methods provide unparalleled resolution for identifying the molecular underpinnings of bilayer energetics. To take advantage of these simulations, new tools must be generated to efficiently identify novel lipid pairs and analyze their per-lipid continuum properties.

To accomplish this, we developed a novel analysis that uncovers the properties of collections of lipids, including dimers. The analysis takes two approaches to isolating important dimer structures. The first directly identifies dimers that contained features suspected to be strong, such as salt-bridged interactions and hydrogen bonding. The second, a hidden Markov model (HMM), allows for the emergence of structural features based on their similarity in space and time. We consider this approach to be "semi-automated" in that the important lipid sites were chosen (e.g., charged moieties, hydrogen-bond donors) as structural information but were not enforced to map to states.

Markov models have shown promise in being able to extract mechanistic insight and timescale information from molecular simulations. The Markov model framework provides a formalism for defining timescales for processes (31). It typically relies on a discrete assignment of state such that transitions between states can be counted. They have been successfully employed to study several problems in molecular biophysics, including protein folding (32–36), ligand binding (37), protein-protein associations (38), and phase identification in lipid bilayers (39).

HMMs allow for a weak association of an observable and the state of interest. In an HMM, there is not a one-to-one mapping of an observation to state. Rather, observed configurations are assigned to a state based on the time sequence of observations. Applications to lipid bilayers are particularly amenable to HMM analysis. First, the large number of target molecules in a simulation is directly proportional to the sampling statistics that can be obtained through simulation. In simulation systems containing hundreds of lipid molecules, even somewhat rare states can be sampled. Second, the molecular environment around a lipid relaxes much more slowly than for material solvated by water. This strongly suggests a hidden contextual influence on lipid configuration.

In this work, we use three unique test cases to examine varied effects of lipid-lipid interaction on the preferred curvature (spontaneous curvature) of lipid dimers. In order to better control for bilayer effects, we have chosen to simulate only symmetric bilayers. We introduce the additive model as the null hypothesis to which we compare dimer curvature preference. Subconformations of lipid dimers that exhibit non-additive spontaneous curvatures are then identified as curvature-sensitive states. In all cases, curvature-sensitive states were most easily identified by standard interaction metrics (e.g., hydrogen-bond formation and divalent-cation binding). These were predominantly distance-based cutoffs for chemical sites known to form relatively strong interactions. The three systems studied with the approach were 1) a tertiary mixture of DOPC, 1,2-dioleoyl-sn-glycero-3-phosphoethanolamine (DOPE), and 1,2-dioleoyl-sn-glycero-3-phospho-L-serine (DOPS), 2) a mixture of phosphatidyl-inositol-4,5-bisphosphate (PIP2) and 1-palmitoyl-2-oleoyl-glycero-3-phosphocholine (POPC), and 3) binary mixtures of PSM and POPC. These three mixtures highlight three unique mechanisms that can alter the spontaneous curvature of a dimer conformation. Specifically, the DOPC, DOPE, and DOPS system illustrates the impact of hydrogen-bond formation on the negative spontaneous curvature of PE. The more physiologically relevant systems (2 and 3) help to provide mechanistic insights into lipid-lipid interactions that are important for cellular function. We observed that Ca^{2+}-meditated heterodimers between PIP2 and POPC have highly negative spontaneous curvature. The implication is that curvature generation by PIP2 does not require clustering. Additionally, the PSM and POPC mixtures reveal a complicated role for hydrogen bonding that alters dimer spontaneous curvature in a way that appears to depend on the lipid matrix. As PSM is a major component in the plasma membrane and has been observed in nanometer-scale domains in cells (40), this finding has potentially broad-reaching implication for a number of membrane trafficking processes that depend on membrane mechanics.

METHODS

Molecular dynamics

Build and simulation parameters

All simulations used the CHARMM C36 lipid force field (41). Both PC/PE/PS and PSM/POPC simulations were built to be oblong, with one lateral dimension four times larger than the other, to capture long wavelength undulations. Simulations of PIP2/POPC were built square. While the simulations made with oblong geometries provide access to longer wavelengths, the differences in geometry of these systems do not impact the mechanical properties extracted from our simulations. Four replicas of PC/PE/PS each had 1272 total lipids. One replica each of 10%, 20%, or 30% PSM in POPC had 1320 total lipids. One simulation of 10:1 PIP2:POPC had total 484 lipids, with 129 Ca^{2+} ions. When simulating PIP2, the CHARMM residues SAPI24 and SAPI25 were used in equal amounts. The residues only vary by the protonation state of either the fourth or fifth position phosphate group. These lipids both possess one stearoyl (18 carbon, fully saturated) and one arachidonic (20 carbon, 4 unsaturated bonds) acyl tail each. All systems were simulated for at least one microsecond (summing all replicas) with a constant temperature of 310.15 K and pressure of 1 bar. A summary of components and durations for each of the simulation systems is listed in Table S5.

Using NAMD (42), systems were minimized and initially relaxed as prescribed by CHARMM-GUI. After these steps, the systems were converted into AMBER format (43,44) using ParmEd. All analyzed data was simulated with AMBER. Constant temperature was targeted and regulated by a Langevin thermostat with a friction coefficient of 1 ps^{-1}, and constant pressure was anisotropically (x and y coupled; zero surface tension) maintained by a Monte Carlo barostat. Note that there was no apparent static buckling of the membrane as observed in ref. (45). Nonbonded interactions were switched off between 10 and 12 Å using force-based switching. Long-range electrostatics were handled by the PME implementation for GPUs by Salomon-Ferrer et al. (46). The PME grid was constructed with a spacing of less than 1 Å (tolerance = 10^{-5}; Ewald coefficient = 0.22664; inter-polation order = 4). Bond lengths involving hydrogen were constrained by SHAKE (47); water was kept rigid using SETTLE (48). A 2 fs time step was used, and coordinates were saved every 200 ps for analysis.

Dimer identification

Lipid structures were characterized by a subset of atoms, defined for each type below. Pairs of lipids were selected if the center of geometry of the subset was within 14 Å. Atom names are listed below in the C36 lipid force field naming scheme.

Hydrogen bonding from DOPE

The atom selections for DOPE, DOPC, and DOPS were {P, N, C1, C3, C24, and C34}. Hydrogen bonds between lipids were identified when a PE hydrogen was within 2.5 Å of a hydrogen-bond acceptor, here either the phosphate oxygens or the carbonyl oxygens.

Divalent-cation mediation of PIP2

Both SAPI24 and SAPI25 PIP2 residues were treated identically in lipid-pair detection. The atom selections for PIP2 were {C11, C12, C13, C14, C15, C16, P4, P5, P, C1, C2, C3, C21, and C31}, while POPC used {P, N, C1, and C11}. Divalent-cation-mediated dimers were identified when a Ca^{2+} (or Mg^{2+}; see supporting material) ion was within 4 Å of the center of geometry of a lipid dimer.

Hydrogen bonding of PSM

The atom selections for PSM were {N, P, NF, HNF, O3, HO3, and OF}. Hydrogen bonds between lipids were identified when either the HNF or HO3 atom was within 2.5 Å of a hydrogen-bond acceptor, here a phosphate oxygen, OF, or O3.

General state identification with an HMM

The full description of the HMM methodology for dimer state extraction is described in the supporting material. Briefly, a subset of dimer states was extracted using the atom selections and cutoffs above, yielding between 10^4 and 2×10^4 structures for a dimer type. Fifty-two clusters were formed by K-medoid clustering, which chooses clusters based on representative structures from a set, associating each member of the whole set with a cluster center to minimize the summed root-mean-square deviation of the clusters. These clusters formed the observable in the HMM. Following the definition of the clusters, all time-ordered sequences of dimers were extracted from the simulation, assigning each instance of a dimer to a cluster based on root-mean-square deviation. An HMM describing the observed sequences of dimer clusters was created by optimizing the transition and observation probabilities of the HMM such that the probability of observing the ordered sequences was maximized. State was then assigned to each dimer configuration based on the optimized HMM.

Computation of dimer curvature preference

We define here the curvature-coupled redistribution (CCR) method, which extracts the curvature experienced by lipids, implying the spontaneous curvature (21). A cartoon illustrating the overall approach is shown in Fig. 1.

The instantaneous (i.e., per frame) discrete Fourier spectrum is computed on a grid with maximum spacing of 15 Å. The height is computed first for each leaflet; the bilayer height is the mean of the two. The coefficient $h_{\mathbf{q}}$ of mode q is

$$h_{\mathbf{q}} = \sum_i h_i e^{i\mathbf{q}\cdot\{x_i,y_i\}}, \tag{3}$$

where here h_i is the height of the grid point located at lateral coordinates $\{x_i, y_i\}$. For each frame in the trajectory, the set $\{h_{\mathbf{q}}\}$ is recorded, along with the lateral $(\{x, y\})$ positions for each lipid.

The instantaneous curvature a lipid experiences is computed as $-\nabla^2 h(x, y)$:

$$c(x, y) = \sum_{q_{\min}}^{q_{\max}} h_{\mathbf{q}} |\mathbf{q}|^2 e^{i\mathbf{q}\cdot\{x,y\}}, \tag{4}$$

which is real as $h_{\mathbf{q}} = h^*_{-\mathbf{q}}$. The upper cutoff, $q_{\max}$, determines the highest frequency mode used to compute curvature. In this analysis, lower q modes are less well sampled because they occur more slowly. Conversely, higher q modes are more readily sampled, helping to reduce error in the calculations. The cost of including these high q modes is the potential biasing of the analysis to only describe these short wavelength fluctuations instead of the whole bilayer. The $q_{\max}$ used in our analysis 0.08 attempts to balance these considerations. The average curvature, $(\langle c \rangle)$, experienced by a lipid is then the average of $c(x, y)$ over the trajectory.

Lipids can be analyzed as monomers to determine single-lipid spontaneous curvature as pairs (e.g., DOPE-DOPE homodimers or POPC-PIP2 heterodimers) or as subsets of lipid pairs differentiated by a specific chemical interaction (e.g., hydrogen-bond formation or ion binding). Lipid populations will be compared in terms of their experienced curvature, $\langle c \rangle$, calculated using Eq. 4 and averaged over the duration of the simulation. The quantity $\langle c \rangle$ is directly proportional to spontaneous curvature (c_0). The benefit of using $\langle c \rangle$ is that it can be directly calculated from simulation and does not rely on knowledge of the area per lipid in a complex. An additive model is useful as the null hypothesis of a single-lipid c_0; it accounts for the likelihood of finding two curvature-sensitive lipids co-localized. Subpopulation $\langle c \rangle$ can then be compared with each other as well as with the additive model.

The additive model for lipid dimers

A simple hypothesis for the spontaneous curvature of dimers is that their spontaneous curvature is the area-weighted average of the two species and that the total area of the dimer is the sum of the monomer areas:

$$\begin{aligned} c_{0,\mathrm{A+B}} &= \frac{A_{\mathrm{A}} c_{0,\mathrm{A}} + A_{\mathrm{B}} c_{0,\mathrm{B}}}{A_{\mathrm{A+B}}} \quad \text{(additive approximation)} \\ A_{\mathrm{A+B}} &= A_{\mathrm{A}} + A_{\mathrm{B}}. \end{aligned} \tag{5}$$

From the Helfrich/Canham model (26,27) and assuming a localized lipid mechanical extent (21), the experienced curvature of some embedded molecule x on mode q is proportional to its area fraction ($\frac{A_x}{A}$, where A_x is the area of the embedded object and A is the area of the bilayer patch) times its spontaneous curvature difference with the background, Δc_0 (21):

$$\langle c_{\mathrm{x}} \rangle = \frac{A_{\mathrm{x}}}{A} \Delta c_{0,\mathrm{x}}. \tag{6}$$

The additive model of two interacting lipids is that the experienced curvature for a dimer ($\langle c_{\mathrm{A+B}} \rangle_{\mathrm{additive}}$) is the sum of the observed monomer curvatures:

$$\begin{aligned} \langle c_{\mathrm{A+B}} \rangle_{\mathrm{additive}} &= \frac{A_{\mathrm{A+B}}}{A} \frac{A_{\mathrm{A}} \Delta c_{0,\mathrm{A}} + A_{\mathrm{B}} \Delta c_{0,\mathrm{B}}}{A_{\mathrm{A+B}}} \\ &= \frac{A_{\mathrm{A}}}{A} \Delta c_{0,\mathrm{A}} + \frac{A_{\mathrm{B}}}{A} \Delta c_{0,\mathrm{B}} \\ &= \langle c_{\mathrm{A}} \rangle + \langle c_{\mathrm{B}} \rangle. \end{aligned} \tag{7}$$

Our methodology distinguishes the case that interacting lipids (e.g., hydrogen-bonded PE lipids) have a unique spontaneous curvature from the null hypothesis that random co-localization of curvature sensitive lipids doubles the monomer effect. In both cases, the background is the average c_0 of the complete bilayer, where Δc_0 is the difference of the target lipid (e.g., a PE monomer or dimer) relative to all the lipids, including PE. The additive model assumes that the spontaneous curvature of the PE lipids is constant, regardless of its environment. To characterize interacting lipids, we compare the experienced curvature of all PE-PE pairs that form a hydrogen bond between lipid headgroups with the additive model. This comparison is possible because the CCR method can track lipids that have been tagged in specific states. If the formation (or lack of) hydrogen bonds influences the curvature preference of interacting lipids, it will manifest as the lipid subpopulation having a significantly different experienced curvature than that of non-interacting lipids. These two cases illustrate how the CCR method can be used to investigate the molecular mechanisms that drive spontaneous curvature.

The additive model may overestimate the spontaneous curvature of a monomer due to attractive interactions between lipids. That is, the

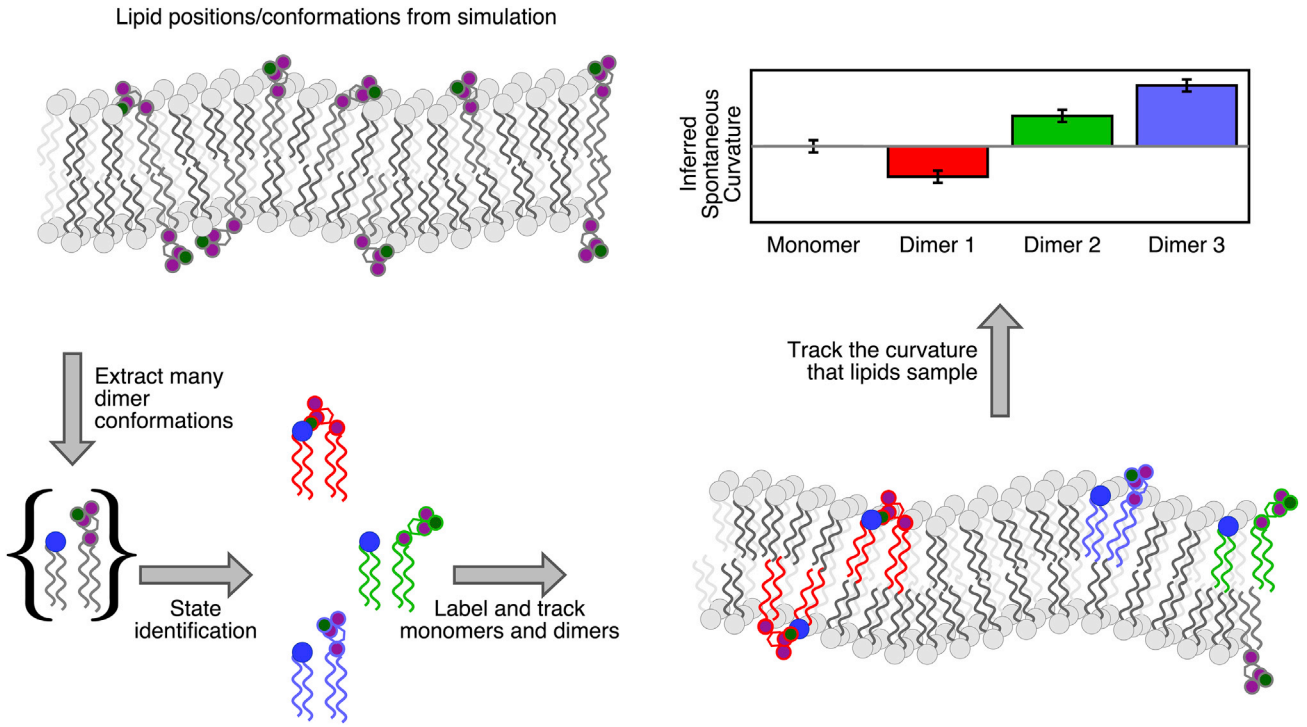

FIGURE 1 A cartoon illustrating the curvature-coupled redistribution method. Beginning at the top left and proceeding counter-clockwise, a patch of multicomponent bilayer is simulated (represented above by *purple and gray lipids* in the *top left*). A set of dimer conformations are extracted and collected into states with common properties. Here, the cartoon represents divalent-cation-mediated interactions between an anionic lipid and its neighbors. The correlation of state (i.e., molecular structure) and curvature is recorded and compared with Helfrich/Canham theory. The mechanism of curvature sensitivity of a state is inferred from the correlation of structure and sampled curvature. To see this figure in color, go online.

monomer may appear to have a stronger influence on curvature because its effect is amplified by co-localization.

The additive model as the null hypothesis

All three test systems described above are analyzed using the same relative reference state: the additive model. The Δc_0 used to construct the model comes from the bulk lipid redistribution analysis and are reported as the single lipid species differences in spontaneous curvature. Values of Δc_0 for each monomer in this paper are reported in Table 1. Use Eq. 7 to translate between Δc_0 and experienced curvature, $\langle c \rangle$.

Dimer spontaneous curvature is distinguished by comparison with lipid monomers. Monomers are defined as those lipids that do not meet the criteria for a dimer. For example, when classifying PIP2-PIP2 dimers, PIP2 lipids as members of PIP2-Ca^{2+}-POPC complexes would be classified as monomers if they are not in complex with other PIP2 lipids. When identifying PIP2-Ca^{2+}-POPC complexes, PIP2 lipids as members of PIP2-PIP2 complexes would be classified as monomers if they are not bridged by Ca^{2+} to POPC.

RESULTS

Hydrogen-bond donation from DOPE lipids induces negative curvature

Fig. 2 reports the average curvature experienced by dimers of DOPE with DOPE, DOPC, or DOPS. The simulations in this work have been previously used in ref. (21) to establish the equivalence between the lateral pressure profile and CCR methodology. It is clear that DOPE modeled with the CHARMM C36 force field has a negative spontaneous curvature, consistent with experiment (28). Also apparent from this analysis is the observation that complex formation with DOPE leads to significant deviations from the additive approximation.

The spontaneous curvature of lipid dimers containing DOPE depends on variations of the intra-complex conformations of interacting lipids. Two mechanisms are proposed to influence the spontaneous curvature of DOPE: headgroup

TABLE 1 Δc_0 values used in the additive model

Lipid	Δc_0 ($Å^{-1}$)	Simulation
DOPE	-0.015 ± 0.002	30% DOPE 25% DOPC +45% DOPS
DOPC	$+0.010 \pm 0.002$	
DOPS	$+0.003 \pm 0.001$	
PIP2	-0.028 ± 0.006	10% PIP2 90% POPC
POPC	$+0.004 \pm 0.001$	
PSM	-0.001 ± 0.002	10% PSM 90% POPC
POPC	$+0.003 \pm 0.0002$	
PSM	$+0.001 \pm 0.0009$	20% PSM 80% POPC
POPC	-0.0002 ± 0.0002	
PSM	$+0.003 \pm 0.0006$	30% PSM 70% POPC
POPC	-0.0005 ± 0.0002	

These Δc_0 values are calculated from a bulk analysis of spontaneous curvature values for individual lipid species subtracted from the spontaneous curvature of the entire membrane. Error bars represent one standard error of the mean (SEM).

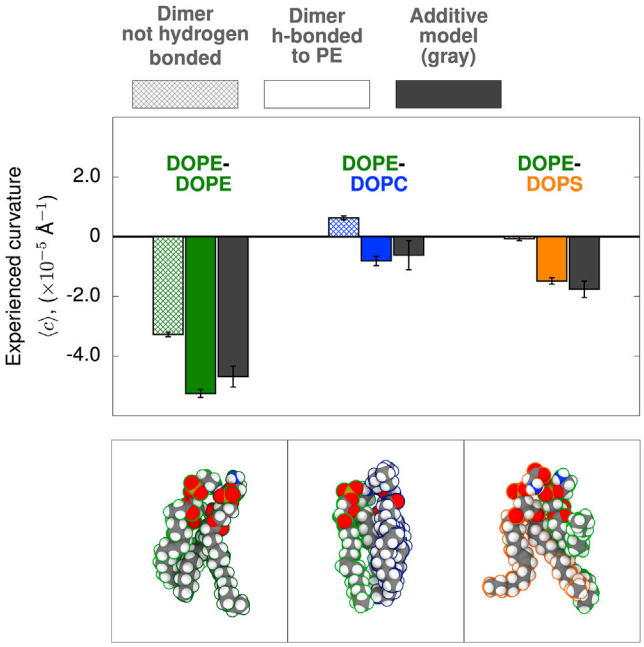

FIGURE 2 Hydrogen-bond donation from PE headgroups enhances negative curvature in lipid dimers. Legend above figure (in *gray*) shows the crosshatched bars that represent the non-hydrogen-bonded complexes, the colored bars represent the hydrogen-bonded dimers, and the gray bar represents the theoretical, additive model. Experienced curvature is plotted for lipids as monomers or as in complex. Lipids (DOPE, *green*; DOPC, *blue*; DOPS, *gold*) are colored by type. The additive model is shown in gray. The bottom panels are representative molecular configurations of hydrogen-bonded dimers. To see this figure in color, go online. Error bars represent one SEM.

size and hydrogen-bond formation (49–51). The small PE headgroup suggests that it is a predominant factor in determining its negative spontaneous curvature. The present analysis indicates, however, this is not the complete story. A comparison of dimers in which DOPE forms a hydrogen bond (Fig. 2, *middle column, solid*) or does not (Fig. 2, *left column, hashed*) indicates substantially increased negative spontaneous curvature for configurations with hydrogen bonding. In all three cases, the statistical significance of experienced curvature differences between the states as determined by pairwise comparison indicates a significant difference between the non-hydrogen-bonded and hydrogen-bonded dimer states: DOPE-DOPE ($p = 0.000077$), DOPE-DOPC ($p = 0.0011$), and DOPE-DOPS ($p = 0.000083$). Complete tables of p values can be found in the supporting material. This highlights the importance of specific molecular interactions when relating lipid content to curvature.

Following theory (Eq. 1), this system should undergo both diffusional and conformational softening. DOPE can form complexes between all three types of lipids in the system, each with a different bulk curvature preference. The dynamic, diffusional coupling of these complexes to membrane undulations will lower the apparent bending modulus. Likewise, formation of a hydrogen bond in each of these complexes significantly changes c_0 to become more negative. Rapid inter-conversion between these states then leads to a softer bilayer. Even in a system with only three components, lipid heterogeneity and molecular details complicate the traditional continuum interpretation of bilayer mechanics.

Divalent-cation-mediated interactions of PIP2 induce negative curvature independent of clustering

Three PIP2 dimer schemes were analyzed. In the first, a dimer is defined by its interactions with neighboring PIP2 (Fig. 3, *left column*). Redistribution analysis indicated dimers were consistent with twice the monomer model (compare twice the value of the striped bar and the crosshatched bar, $\langle c_{\mathrm{dimer}}\rangle = (1.9 \pm 0.5)\langle c_{\mathrm{monomer}}\rangle$ when compared at $p = 0.05$). Thus, PIP2-PIP2 interactions did not appear to influence curvature. Second, PIP2-PIP2 dimers were isolated if their interaction was mediated by Ca^{2+} (Fig. 3, *center column*). Ca^{2+} interactions within the dimer showed no significant changes in negative curvature (Fig. 3, *solid purple and crosshatched bars*; $p = 0.15$). Third, the dimer state was defined as a Ca^{2+}-mediated interaction with neighboring POPC (Fig. 3, *right column*). Here, a significant, non-additive negative curvature preference was detected (Fig. 3, *solid purple to gray*; $p = 0.0093$). Note that Ca^{2+}-mediated clustering of PIP2 has likely led to an overestimate of the PIP2 monomer spontaneous curvature, yielding a dimer additive model that overestimates the effect of a dimer (Fig. 3, *first and second columns*).

These results support current models of PIP2 cluster curvature preference and highlight the need to better understand the role of divalent cations in mediating PIP2 heterodimer formation. While in native membranes PIP2 is a minor lipid species (52), it can form clusters that enhance local concentration (53). In this case, the PIP2 clusters should act as a slowly diffusing curvature-sensitive inclusion that contributes to softening. While the PIP2-PIP2 interactions within the clusters may not show a strong preference for negative curvature, these clusters are also surrounded by a myriad of other lipids. Our results suggest that further analysis of PIP2 clustering would show that curvature is affected by the boundary of a PIP2 domain, where conformations would more closely resemble the PIP2-Ca^{2+}-POPC interaction we identify. These types of ion-mediated heterodimers present a potentially important case for conformational softening near PIP2 clusters that may have functional relevance for curvature-influencing proteins that bind PIP2 (4).

PSM complex formation promotes positive curvature

Fig. 4 shows that the monomeric state of PSM exhibits similar curvature preferences to POPC (little net curvature

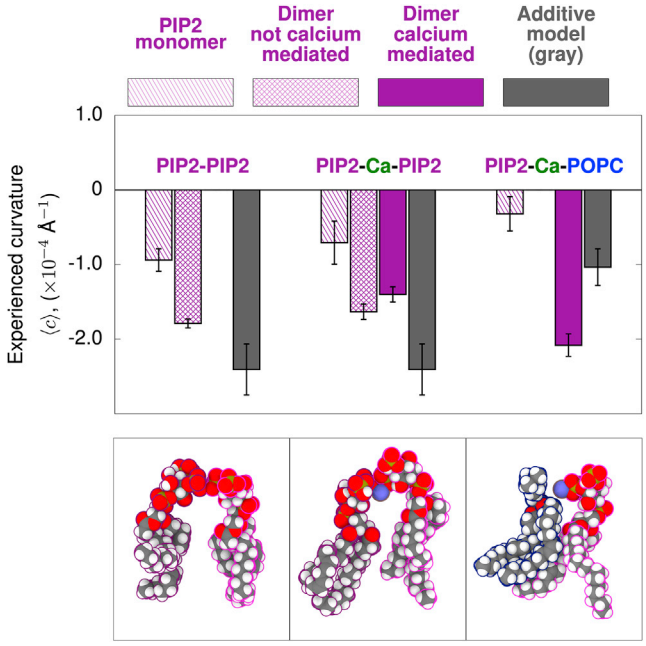

FIGURE 3 Calcium-bridged interactions between PIP2 and POPC show strong negative curvature. Experienced curvature is plotted for lipids as monomers or as in complex. The additive model is shown in gray, and monomers are striped. Dimers are crosshatched. Ca^{2+}-mediated dimers are solid. The bottom panels are representative molecular configurations of each type (PIP2-PIP2, PIP2-Ca^{2+}-PIP2, and PIP2-Ca^{2+}-POPC). To see this figure in color, go online. Error bars represent one SEM.

preference). Neighboring PSM lipids without hydrogen bonds do not show a positive curvature preference (Fig. 4, *crosshatched bars*). By comparison, PSM lipids that form amide-mediated hydrogen-bonded states exhibit a positive spontaneous curvature (Fig. 4, *solid bars*). This shift to a more positive spontaneous curvature becomes more pronounced as the mole fraction of PSM is increased. At 30 mol % fraction of PSM, the experienced curvature difference between dimer states with and without hydrogen bonds becomes statistically significant ($p = 0.0038$). The p values comparing the other states in this analysis can be found in Table S4. The relationship between the increased positive curvature preference of the hydrogen-bonded state and the mol fraction of PSM suggests that formation of the amide hydrogen bond helps to drive shift to more positive spontaneous curvature at higher concentrations of PSM.

It is important to highlight that hydrogen-bond formation in the PSM systems has the opposite effect (i.e., biasing the complex to more positive curvatures) that what was seen in the DOPE system (more negative curvature bias). The positioning of the PSM amide hydrogen bond within the leaflet is likely important for determining the sign of the curvature. Hydrogen-bond formation occurs closer to the bilayer midplane in the PSM lipids than the hydrogen bonds made by lipids PE headgroups. In the case of DOPE, attractive forces near the headgroup surface lead to negative curvature (54). We propose that amide HB formation observed in the PSM system helps to reduce tail entropy and, therefore, shift the curvature preference more positive (further explained in the discussion).

PSM exhibits a concentration-dependent positive curvature preference, yet it is unclear whether the amide-hydrogen-bonded dimer is sufficient to completely explain the trend. We speculate that the increasing positive curvature of PSM is also due to higher-order effects beyond dimerization. For example, with sufficient PSM nearby, cohesive hydrogen bonding supports chain ordering, further lessening entropic tail repulsion and thus its contribution to positive curvature. A similar effect was observed with the chain-ordering ability of cholesterol (30). The possibilities for extending the CCR analysis to higher-order complexes are discussed below.

This system shows an additional way that heterogeneous lipid composition can complicate the traditional continuum view of mixed bilayers. In this case, changes in the lipid matrix composition influence both the sign of different PSM-PSM complex curvature preference and the magnitude of hydrogen-bond formation on the curvature. By making the difference in curvature preferences between the hydrogen-bonded and non-hydrogen-bonded states larger, the anticipated magnitude of conformational softening will increase. Further, as matrix PSM increases, PSM-PSM dimers prefer more positive curvature, which changes where these

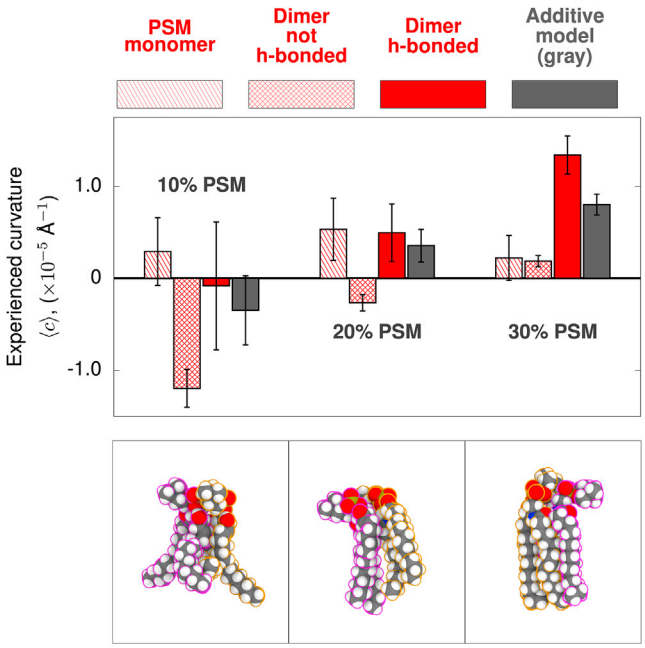

FIGURE 4 Curvature sensitivity of PSM dimers changes with hydrogen-bond formation and concentration. Experienced curvature is plotted for lipids as monomers or as in complex. The additive model is shown in gray, and monomers are striped. Dimers are crosshatched. Hydrogen-bond-mediated dimers are solid. The bottom panels are representative molecular configurations of the amide-hydrogen-bonded configuration. To see this figure in color, go online. Error bars represent one SEM.

structures will diffuse to and will alter the impact of diffusional softening.

DISCUSSION

Curvature preference is a balance of repulsive and cohesive forces along the bilayer normal

Curvature preference is typically described using the heuristic of "lipid shape" that conveniently describes lipids as cones or cylinders (55). Needless to say, specific interactions between lipids are incompatible with shape. Thus, identification of the curvature sensitivity of specific interactions coupling to curvature refutes the ubiquity of the shape model. In contrast, CCR provides the required framework for distinguishing the molecular mechanisms of spontaneous curvature quantitatively.

It is the balance of repulsive and attractive forces that determines the curvature stresses of a leaflet and thus its spontaneous curvature. Qualitatively, repulsive forces originating from bulky headgroups and tail entropy are the essence of the shape model. Attractive forces, such as hydrogen bonding and Coulombic interactions, are better described by specific interactions. Both are quantified in the lateral pressure profiles (54) that are typically used to infer c_0. The lateral pressure profile of PE, for example, has a cohesive stress at the depth of the hydrogen bond (56), relative to PC. There is currently no method to determine, from the pressure profile, whether this is due to the size of the headgroup or hydrogen bonding.

Applying the CCR method allows us to correlate molecular interactions with curvature and make connections to the transverse positions of interactions. In the cases of both DOPE and Ca^{2+}-mediated interactions of PIP2, attractive interactions near the level of the glycerophospholipid phosphate induce strong negative curvature. In contrast, the amide hydrogen bond is formed deeper in the membrane for PSM-PSM dimers. By anchoring the two lipids closer to the tails, we speculate that the hydrogen bond restricts the tail entropy and, therefore, reduces the repulsive forces on that region of the lipid. Lessening the tail repulsion would then give rise to the positive curvature preference of these PSM dimers. Additionally, positive curvature coincides with ordering of the surrounding matrix. That is, c_0 is more positive at 30% PSM, and ordered configurations are likely.

Curvature-dependent lipid configurations determine the bending modulus

The bending modulus κ_b is the elastic constant describing the second-order variation in the curvature energy. The magnitude of κ_b is related to the conformational plasticity of the lipids. An example of this is the stiffening (~5 times (57)) of ordered phase bilayers compared with disordered bilayers. In the liquid disordered phase, lipids are less tightly packed and can adopt a greater range of conformations, presumably leading to a smaller bending modulus. Conversely, the liquid-ordered phase restricts lipid dynamics and increases packing, increasing the bending modulus. The differences between these two phases highlights the importance of molecular details when interpreting a bulk phenomenon like bending energy. We relate two mechanisms of bilayer softening that are displayed on very different timescales. First, consider diffusional softening, the change in the undulation relaxation spectrum due to dynamic lateral fluctuations of a mixture of lipids with varied c_0. The second mechanism shows how membrane bending rigidity can be reduced through the inter-conversion between lipid pairs with distinct, curvature-dependent states, which we refer to as conformational softening. The observed softening generated by both mechanisms is described by Eq. 2. For clarity, we will the specify softening mechanism by denoting α as either α_{diff} or α_{conf}.

Diffusional softening

A bilayer is assembled with symmetrical leaflet composition: a small molecular fraction χ of a lipid species A with spontaneous curvature c_A amid a background of lipids with zero spontaneous curvature. Further assume that there is a well-defined bending modulus κ_b that is the same for the background as well as that of l_A. The bending modulus $\kappa_b^{\mathrm{app.,diff.}}$ of the entire mixture will appear to be

$$\kappa_b^{\mathrm{app.,diff.}} \approx \left[1 - \alpha_{\mathrm{diff}}\right]\kappa_b, \tag{8}$$

with α_{diff} having the same form defined in Eq. 2. Here Δc_0 is the difference of spontaneous curvature between c_A and the spontaneous curvature of the background lipid composition. The softening factor (α_{diff}) arises from the coupling of the lateral distribution of lipids to bilayer undulations. Note that the lateral distribution of lipids relaxes slowly (as $D^{-1}q^{-2}$, where D is the diffusion constant, and $q = \frac{2\pi}{\lambda}$, where λ is the undulation wavelength) for submicron wavelength undulations. This introduces kinetics as an important consideration when investigating softening mechanisms.

Conformational softening

Consider now softening due to (perhaps rapidly) interchanging curvature-dependent conformations. Our results show that different conformations can exhibit different curvature preferences. We have introduced the softening factor α in Eq. 2 that shows mathematically how different curvature-sensitive conformations can soften bilayers. Below, we will provide an additional way to understand this mechanism by how α_{conf} can alter the energy required to bend membranes. We propose a simple model in which mechanical properties (spontaneous curvature and bending modulus) are altered by adding in a specific interaction. The hydrogen bond donated by a PE lipid to a neighbor adds negative curvature preference that appears to be largely

independent of the acceptor (Fig. 2). The Ca^{2+}-mediated interaction between PIP2 and POPC dramatically shifts curvature to be negative (Fig. 3). We model the interacting state as being "added on" by shifting the spontaneous curvature of a reference lipid, such as POPC, by δ. The reference lipid has area per lipid A_R, spontaneous curvature $c_{0,R}$, and bending modulus κ_b. The likelihood of the interacting state is further characterized by its curvature-independent mole fraction, χ.

Apply separate local Helfrich models $H_{ref.}$ and $H_{int.}$ for the curvature energy of the reference and interacting states, respectively:

$$H_{ref.} = \frac{A_R \kappa_m}{2}(c - c_{0,R})^2 \tag{9}$$

and

$$H_{int.} = \frac{A_R \kappa_m}{2}(c - c_{0,R} - \delta)^2, \tag{10}$$

where A_R is the area per lipid for the reference, c is the curvature local to the lipid, and κ_m is the monolayer bending modulus. The free energy (F) is

$$\begin{aligned} F = & -k_B T \log\left((1-\chi)\exp\left(-\frac{H_{ref.}}{k_B T}\right)\right. \\ & \left. + \chi \exp\left(-\frac{H_{int.}}{k_B T}\right)\right). \end{aligned} \tag{11}$$

F can be restructured in a form resembling the Helfrich Hamiltonian. Consider the case in which δ is small. Expanding to second order in δ

$$\begin{aligned} F \approx & A_R \frac{[1-\alpha_{conf}]\kappa_m}{2}(c - c_0')^2 \\ c_0' \approx & c_{0,R} + \delta\chi, \end{aligned} \tag{12}$$

where α_{conf} has the same form outlined in Eq. 2. Because both conformational and diffusional softening have the same factor, $\alpha(\delta,\chi)$, compositional and conformational heterogeneity have a similar effect on bilayer properties. For $\delta = 0.03$ Å^{-1}, $A_p = 65$ Å^{-2}, $\chi = 0.5$, and $\kappa_m = 7$ kcal/mol, the lipid patch has 83% the stiffness. This is a substantial decrease in the apparent stiffness of the bilayer and can be directly attributed to the ability of specific states to stabilize different curvatures.

Unlike chemical composition, the conformational composition fluctuates rapidly. Furthermore, the interchange of conformations is typically much faster than the lateral rearrangement of lipids. An intuitive example is conformational isomerization of acyl chains, which occurs on the subnanosecond timescale (58), whereas lipids require tens of nanoseconds to change neighbors and $D^{-1}q^{-2}$ for a fluctuation with wavenumber q to relax (microseconds for a tens of nanometers lengthscale).

Molecular configurations of lipids are a continuum, not discrete. The reasoning in this section thus only forms a rationale for how curvature sensitivity of conformational sets determines softening rather than for predicting κ_b *ab initio*. We have implicitly chosen κ_b to represent the bending modulus of some idealized simple lipid, for example, POPC, that serves as a base value. Stiffening, on the other hand, may result in the removal of conformational space, for which the base of κ_b of POPC, and the treatment here would be inadequate.

Impact of timescale on membrane elasticity measurements

The impact of two complementary but temporally distinct mechanisms for bilayer softening should be observable by techniques that measure κ_b. Equilibrium measurements that report the entire distribution of undulation amplitudes (diffusive x-ray studies and fluctuation analysis) will show the effects of both diffusion and conformational softening. The apparent bending modulus $\kappa_{app.}$ measured using these techniques likely best models the average work required to deform a membrane.

By comparison, experiments that infer mechanical properties from relaxation kinetics can shed light on complex mechanisms that underly mechanics. Neutron spin echo (NSE) and nuclear magnetic resonance spectroscopies will be influenced by the fast relaxation processes that determine conformational softening. Where only the faster relaxation times of short wavelength undulations are probed, mechanical properties will be insensitive to diffusional softening.

How these two softening mechanisms intersect and impact membrane mechanics highlights the importance of considering timescales and length scales when measuring membrane elasticity. Consider the NSE and nuclear magnetic resonance experiments on mixtures of DOPC and cholesterol in ref. (59), which find that a DOPC bilayer is stiffened by cholesterol. Diffusional softening is expected by cholesterol, a lipid that induces high negative curvature (28), yet this would only be clear from techniques able to probe long timescales in which lateral fluctuations of cholesterol concentration are relaxed. This is a plausible explanation for the disagreement between diffusive x-ray studies and NSE techniques (60,61). Combining the two techniques would isolate mechanisms of softening that are important at separate timescales and increase clarity into the molecular impact of cholesterol on membrane mechanics.

Impact on bilayer viscosity

The undulation of a simple bilayer relaxes with rate $\frac{\kappa_b q^3}{4\eta}$ at low q, where η is the solvent viscosity (62). For higher

frequency undulations occurring on the submicrometer length scale and submicrosecond timescale, inter-leaflet friction and surface viscosity slow the relaxation rate (63). Experimental work using homogeneous PC lipid bilayers suggest that acyl chain dynamics are important determinants of viscosity (64). Extending insights drawn from bulk alkane systems (65), the authors speculate that both internal dynamics controlled by factors such as tail saturation and external factors (e.g. lipid-lipid coupling) control different timescale relaxation phenomena (64).

In addition to acyl chain dynamics, ensembles of curvature-sensitive conformations must also relax; we hypothesize that the lipids studied herein, as well as others with similar chemistry, should contribute to the viscosity. The lifetimes of complexes studied here (many nanoseconds for PIP2-Ca^{2+}-POPC bridging) are on the same order of magnitudes for the slow relaxation times reported in studies of alcohol and alkane systems (65) and DMPC bilayers (64). Plausibly, long-lived lipid dimers would increase the lipid-lipid couplings that are proposed to dominate at higher q. In this way, we identify two competing ways that viscosity can be altered by headgroup dynamics and heterogeneity in multicomponent bilayers (diffusional and conformational). In lieu of the additional molecular mechanism implicated in determining bilayer viscosity, new whole-lipid approaches are needed for investigating the viscoelastic properties of multicomponent bilayers.

Importance of divalent-cation-mediated heterodimers in PIP2 membrane mechanics

The unique chemistry of PIP2 allows it to play an outsized role in healthy cell physiology. Despite being 1% of cellular membrane composition (66), it is an essential part of cellular pathways including actin dynamics, cell adhesion, endocytosis, signaling, and organelle trafficking (67,68). In these processes, PIP2 binds various effector proteins that can either be peripheral membrane proteins (e.g., BAR proteins, kinases, etc.) or integral membrane proteins (e.g., voltage-gated potassium channels). PIP2 function is tied to cellular localization that depends intimately on the physical chemistry of the lipid. It is a negatively charged lipid due to the addition of phosphate groups and, as a result, can make a strong complex with divalent cations but only if the cation is present at sufficient concentration (69).

Divalent-cation binding is important to PIP2 membrane biophysics. Studies have shown that PIP2 organization in lipid bilayers is altered by the presence of divalent cations (70). Namely, PIP2 is suggested to form microdomains within the native membrane and thereby increase its effective local concentration (70). While calcium is a physiologically important ion, clustering also is induced by magnesium and zinc (53). Computational studies have used graph theory and network analysis to describe the differences these various ions have on inter-connectivity induced by these ions (71). Simulations of PIP2 indicate it has negative spontaneous curvature, with divalent-cation binding increasing the coupling to negative curvature (72). This adds an additional layer of complexity to understanding microdomain formation in PIP2. In addition to knowing that PIP2 can exist at high effective concentrations, it is also important to consider the local bilayer structure of PIP2 microdomains.

In ref. (72), the negative curvature of Ca^{2+}-bound PIP2 is studied in pure PIP2 bilayers. The authors found that high calcium concentrations (2:1 Ca^{2+}:PIP2) are necessary to induce the strongest negative curvature. In contrast, we find that at 10% coverage, it is the simple Ca^{2+}-mediated interactions with neighboring POPC that induce negative curvature, an effect that would not be apparent in a bilayer saturated with PIP2. According to our analysis, domains of PIP2 are not required for a profound mechanical effect. Rather, it is the strong connection to neighboring lipids by divalent cations that is required.

CONCLUSIONS

This study introduces methodology for linking molecular interactions to lipid spontaneous curvature. The negative spontaneous curvature of PE lipids is partly explained by its ability to donate hydrogen bonds to neighboring lipids. Divalent-cation-mediated interactions between PIP2 and neighboring glycerophospholipids show a strong trend to negative curvature, indicating that domains of PIP2 are not required for its negative curvature preference. In a third case, hydrogen-bond-linked conformations of PSM showed a strong positive curvature preference only at higher PSM concentrations, suggesting the ordered lipid matrix is part of the mechanism.

The shape of membranes is typically interpreted in terms of the average, or monomer, mechanical properties of lipids, assuming static or uniform distributions of lipids. Biological membranes, however, are neither static nor uniform. By ignoring the possibility of substates with different curvature preferences or averaging over these substates, it is likely that important mechanistic insights into physiological process are being missed. The simulation methodology here presents a path to understanding this complexity, with the mechanism testable by scattering and membrane-fluctuation analysis techniques. In our judgment, the modeling of κ_b with diffusional and conformational softening, the characterization of the spatial mechanical extent of lipids and multilipid complexes (21), and the understanding of the effects of differential stresses between leaflets (73) are forging a clear path to characterization of the bending modulus and curvature stresses of biological membranes with complex composition.

SUPPORTING MATERIAL

Supporting material can be found online at https://doi.org/10.1016/j.bpj.2022.07.036.

AUTHOR CONTRIBUTIONS

H.J.L., K.C.S., and A.J.S designed the research. H.J.L. and A.H.B. performed the simulations. H.J.L., K.C.S., A.H.B., R.A., and A.J.S. wrote the paper.

ACKNOWLEDGMENTS

This work was supported by the intramural research program of the *Eunice Kennedy Shriver* National Institute of Child Health and Human Development (NICHD) at the National Institutes of Health. A.H.B. was supported by a Postdoctoral Research Associate (PRAT) fellowship from the National Institute of General Medical Sciences, award number 1Fi2GM137844-01. R.A. acknowledges support from the National Science Foundation under award number MCB-2137154. Molecular rendering was performed with Tachyon software written by John E. Stone. Simulations were performed on computational resources provided by the NICHD.

DECLARATION OF INTERESTS

The authors declare no competing interests.

REFERENCES

1. Harayama, T., and H. Riezman. 2018. Understanding the diversity of membrane lipid composition. *Nat. Rev. Mol. Cell Biol.* 19:281–296.
2. Dennis, E. A., and P. C. Norris. 2015. Eicosanoid storm in infection and inflammation. *Nat. Rev. Immunol.* 15:511–523.
3. Fernandis, A. Z., and M. R. Wenk. 2007. Membrane lipids as signaling molecules. *Curr. Opin. Lipidol.* 18:121–128.
4. Mandal, K. 2020. Review of PIP2 in cellular signaling, functions and diseases. *Int. J. Mol. Sci.* https://doi.org/10.3390/ijms21218342.
5. Van Meer, G., D. R. Voelker, and G. W. Feigenson. 2008. Membrane lipids: where they are and how they behave. *Nat. Rev. Mol. Cell Biol.* 9:112–124.
6. Lujan, P., and F. Campelo. 2021. Should I stay or should I go? Golgi membrane spatial organization for protein sorting and retention. *Arch. Biochem. Biophys.* 707:108921.
7. Nakamura, M. T., B. E. Yudell, and J. J. Loor. 2014. Regulation of energy metabolism by long-chain fatty acids. *Prog. Lipid Res.* 53:124–144.
8. Deevska, G. M., and M. N. Nikolova-Karakashian. 2017. The expanding role of sphingolipids in lipid droplet biogenesis. *Biochim. Biophys. Acta. Mol. Cell Biol. Lipids.* 1862:1155–1165.
9. Lorent, J. H., K. R. Levental, …, I. Levental. 2020. Plasma membranes are asymmetric in lipid unsaturation, packing and protein shape. *Nat. Chem. Biol.* 16:644–652.
10. Levental, I., and S. Veatch. 2016. The continuing mystery of lipid rafts. *J. Mol. Biol.* 428:4749–4764.
11. Cheng, X., and J. C. Smith. 2019. Biological membrane organization and cellular signaling. *Chem. Rev.* 119:5849–5880.
12. Stone, M. B., S. A. Shelby, …, S. L. Veatch. 2017. Protein sorting by lipid phase-like domains supports emergent signaling function in b lymphocyte plasma membranes. *Elife.* 6:e19891.
13. Soubias, O., W. E. Teague, …, K. Gawrisch. 2010. Contribution of membrane elastic energy to rhodopsin function. *Biophys. J.* 99:817–824.
14. Beaven, A. H., A. M. Maer, …, W. Im. 2017. Gramicidin A channel formation induces local lipid redistribution I: experiment and simulation. *Biophys. J.* 112:1185–1197.
15. Brown, M. F. 2012. Curvature forces in membrane lipid-protein interactions. *Biochemistry.* 51:9782–9795.
16. Steinkühler, J., E. Sezgin, …, R. Dimova. 2019. Mechanical properties of plasma membrane vesicles correlate with lipid order, viscosity and cell density. *Commun. Biol.* 2:337.
17. Gracià, R. S., N. Bezlyepkina, …, R. Dimova. 2010. Effect of cholesterol on the rigidity of saturated and unsaturated membranes: fluctuation and electrodeformation analysis of giant vesicles. *Soft Matter.* 6:1472–1482.
18. Semrau, S., T. Idema, …, C. Storm. 2008. Accurate determination of elastic parameters for multicomponent membranes. *Phys. Rev. Lett.* 100:088101.
19. Needham, D., and R. S. Nunn. 1990. Elastic deformation and failure of lipid bilayer membranes containing cholesterol. *Biophys. J.* 58:997–1009.
20. Leibler, S. 1986. Curvature instability in membranes. *J. Phys. France.* 47:507–516.
21. Sapp, K. C., A. H. Beaven, and A. J. Sodt. 2021. Spatial extent of a single lipid's influence on bilayer mechanics. *Phys. Rev. E.* 103:042413.
22. Kozlov, M. M., and W. Helfrich. 1992. Effects of a cosurfactant on the stretching and bending elasticities of a surfactant monolayer. *Langmuir.* 8:2792–2797.
23. Bivas, I., and P. Méléard. 2003. Bending elasticity and bending fluctuations of lipid bilayer containing an additive. *Phys. Rev. E Stat. Nonlin. Soft Matter Phys.* 67:012901.
24. Tian, A., B. R. Capraro, …, T. Baumgart. 2009. Bending stiffness depends on curvature of ternary lipid mixture tubular membranes. *Biophys. J.* 97:1636–1646.
25. Bashkirov, P. V., P. I. Kuzmin, …, V. A. Frolov. 2022. Molecular shape solution for mesoscopic remodeling of cellular membranes. *Annu. Rev. Biophys.* 51:473–497.
26. Helfrich, W. 1973. Elastic properties of lipid bilayers: theory and possible experiments. *Z. Naturforsch. C.* 28:693–703.
27. Canham, P. B. 1970. The minimum energy of bending as a possible explanation of the biconcave shape of the human red blood cell. *J. Theor. Biol.* 26:61–81.
28. Chen, Z., and R. P. Rand. 1997. The influence of cholesterol on phospholipid membrane curvature and bending elasticity. *Biophys. J.* 73:267–276.
29. Kaltenegger, M., J. Kremser, …, G. Pabst. 2021. Intrinsic lipid curvatures of mammalian plasma membrane outer leaflet lipids and ceramides. *Biochim. Biophys. Acta Biomembr.* 1863:183709.
30. Sodt, A. J., R. M. Venable, …, R. W. Pastor. 2016. Nonadditive compositional curvature energetics of lipid bilayers. *Phys. Rev. Lett.* 117:138104.
31. Chodera, J. D., and F. Noé. 2014. Markov state models of biomolecular conformational dynamics. *Curr. Opin. Struct. Biol.* 25:135–144.
32. Voelz, V. A., M. Jäger, …, V. S. Pande. 2012. Slow unfolded-state structuring in acyl-CoA binding protein folding revealed by simulation and experiment. *J. Am. Chem. Soc.* 134:12565–12577.
33. Voelz, V. A., G. R. Bowman, …, V. S. Pande. 2010. Molecular simulation of ab initio protein folding for a millisecond folder NTL9(1-39). *J. Am. Chem. Soc.* 132:1526–1528.
34. Noé, F., C. Schütte, …, T. R. Weikl. 2009. Constructing the equilibrium ensemble of folding pathways from short off-equilibrium simulations. *Proc. Natl. Acad. Sci. USA.* 106:19011–19016.
35. Lane, T. J., G. R. Bowman, …, V. S. Pande. 2011. Markov State model reveals folding and functional dynamics in ultra-long MD trajectories. *J. Am. Chem. Soc.* 133:18413–18419.
36. Bowman, G. R., and V. S. Pande. 2010. Protein folded states are kinetic hubs. *Proc. Natl. Acad. Sci. USA.* 107:10890–10895.
37. Paul, F., C. Wehmeyer, …, F. Noé. 2017. Protein-peptide association kinetics beyond the seconds timescale from atomistic simulations. *Nat. Commun.* 8:1095.
38. Plattner, N., S. Doerr, …, F. Noé. 2017. Complete protein-protein association kinetics in atomic detail revealed by molecular dynamics simulations and Markov modelling. *Nat. Chem.* 9:1005–1011.

39. Sodt, A. J., M. L. Sandar, …, E. Lyman. 2014. The molecular structure of the liquid-ordered phase of lipid bilayers. *J. Am. Chem. Soc.* 136:725–732.

40. Frisz, J. F., H. A. Klitzing, …, M. L. Kraft. 2013. Sphingolipid domains in the plasma membranes of fibroblasts are not enriched with cholesterol. *J. Biol. Chem.* 288:16855–16861.

41. Klauda, J. B., R. M. Venable, …, R. W. Pastor. 2010. Update of the CHARMM all-atom additive force field for lipids: validation on six lipid types. *J. Phys. Chem. B.* 114:7830–7843.

42. Phillips, J. C., R. Braun, …, K. Schulten. 2005. Scalable molecular dynamics with NAMD. *J. Comput. Chem.* 26:1781–1802.

43. Case, D. A., T. E. Cheatham, …, R. J. Woods. 2005. The Amber biomolecular simulation programs. *J. Comput. Chem.* 26:1668–1688.

44. Case, D. A., I. Y. Ben-Shalom, …, M. K. Gilson. 2018. Amber 2018. University of California.

45. Gomez, Y. K., A. M. Natale, …, M. Grabe. 2022. Taking the Monte-Carlo gamble: how not to buckle under the pressure! *J. Comput. Chem.* 43:431–434.

46. Salomon-Ferrer, R., A. W. Götz, …, R. C. Walker. 2013. Routine microsecond molecular dynamics simulations with AMBER on GPUs. 2. Explicit solvent particle mesh ewald. *J. Chem. Theory Comput.* 9:3878–3888.

47. Ryckaert, J. P., G. Ciccotti, and H. J. Berendsen. 1977. Numerical integration of the cartesian equations of motion of a system with constraints: molecular dynamics of n-alkanes. *J. Comput. Phys.* 23:327–341.

48. Miyamoto, S., and P. A. Kollman. 1992. Settle: an analytical version of the SHAKE and RATTLE algorithm for rigid water models. *J. Comput. Chem.* 13:952–962.

49. Gruner, S. M. 1985. Intrinsic curvature hypothesis for biomembrane lipid composition: a role for nonbilayer lipids. *Proc. Natl. Acad. Sci. USA.* 82:3665–3669.

50. Hamai, C., T. Yang, …, S. M. Musser. 2006. Effect of average phospholipid curvature on supported bilayer formation on glass by vesicle fusion. *Biophys. J.* 90:1241–1248.

51. Sodt, A. J., and R. W. Pastor. 2014. Molecular modeling of lipid membrane curvature induction by a peptide: more than simply shape. *Biophys. J.* 106:1958–1969.

52. Mitchell, K. T., J. E. Ferrell, and W. H. Huestis. 1986. Separation of phosphoinositides and other phospholipids by two-dimensional thin-layer chromatography. *Anal. Biochem.* 158:447–453.

53. Wen, Y., V. M. Vogt, and G. W. Feigenson. 2018. Multivalent cation-bridged PI(4, 5)P2 clusters form at very low concentrations. *Biophys. J.* 114:2630–2639.

54. Szleifer, I., D. Kramer, …, S. A. Safran. 1990. Molecular theory of curvature elasticity in surfactant films. *J. Chem. Phys.* 92:6800–6817.

55. Frolov, V. A., A. V. Shnyrova, and J. Zimmerberg. 2011. Lipid polymorphisms and membrane shape. *Cold Spring Harb. Perspect. Biol.* 3:a004747.

56. Sodt, A. J., and R. W. Pastor. 2013. Bending free energy from simulation: correspondence of planar and inverse hexagonal lipid phases. *Biophys. J.* 104:2202–2211.

57. Baumgart, T., S. Das, …, J. T. Jenkins. 2005. Membrane elasticity in giant vesicles with fluid phase coexistence. *Biophys. J.* 89:1067–1080.

58. Venable, R. M., Y. Zhang, …, R. W. Pastor. 1993. Molecular dynamics simulations of a lipid bilayer and of hexadecane: an investigation of membrane fluidity. *Science.* 262:223–226.

59. Chakraborty, S., M. Doktorova, …, R. Ashkar. 2020. How cholesterol stiffens unsaturated lipid membranes. *Proc. Natl. Acad. Sci. USA.* 117:21896–21905.

60. Nagle, J. F., E. A. Evans, …, R. Dimova. 2021. A needless but interesting controversy. *Proc. Natl. Acad. Sci. USA*. https://doi.org/10.1073/pnas.2025011118.

61. Ashkar, R., M. Doktorova, …, M. F. Brown. 2021. Reply to Nagle et al.: the universal stiffening effects of cholesterol on lipid membranes. *Proc. Natl. Acad. Sci. USA*. https://doi.org/10.1073/pnas.2102845118.

62. Brochard, F., and J. Lennon. 1975. Frequency spectrum of the flicker phenomenon in erythrocytes. *J. Phys. France.* 36:1035–1047.

63. Seifert, U., and S. A. Langer. 1993. Viscous modes of fluid bilayer membranes. *Europhys. Lett.* 23:71–76.

64. Nagao, M., E. G. Kelley, …, P. D. Butler. 2021. Relationship between viscosity and acyl tail dynamics in lipid bilayers. *Phys. Rev. Lett.* 127:078102.

65. Yamaguchi, T., and A. Faraone. 2017. Viscoelastic relaxations of high alcohols and alkanes: effects of heterogeneous structure and translation-orientation coupling. *J. Chem. Phys.* 146:244506.

66. Van Den Bogaart, G., K. Meyenberg, …, R. Jahn. 2011. Membrane protein sequestering by ionic protein-lipid interactions. *Nature.* 479:552–555.

67. Dickson, E. J., and B. Hille. 2019. Understanding phosphoinositides: rare, dynamic, and essential membrane phospholipids. *Biochem. J.* 476:1–23.

68. Krajnik, A., J. A. Brazzo, …, Y. Bae. 2020. Phosphoinositide signaling and mechanotransduction in cardiovascular biology and disease. *Front. Cell Dev. Biol.* 8:595849.

69. Toner, M., G. Vaio, …, S. McLaughlin. 1988. Adsorption of cations to phosphatidylinositol 4, 5-bisphosphate. *Biochemistry.* 27:7435–7443.

70. Levental, I., F. J. Byfield, …, P. A. Janmey. 2009. Cholesterol-dependent phase separation in cell-derived giant plasma-membrane vesicles. *Biochem. J.* 424:163–167.

71. Han, K., A. Gericke, and R. W. Pastor. 2020. Characterization of specific ion effects on PI(4, 5)P2 clustering: molecular dynamics simulations and graph-theoretic analysis. *J. Phys. Chem. B.* 124:1183–1196.

72. Allolio, C., and D. Harries. 2021. Calcium ions promote membrane fusion by forming negative-curvature inducing clusters on specific anionic lipids. *ACS Nano.* 15:12880–12887.

73. Hossein, A., and M. Deserno. 2020. Spontaneous curvature, differential stress, and bending modulus of asymmetric lipid membranes. *Biophys. J.* 118:624–642.

Biophysical Journal, Volume *121*

Supplemental information

Molecular mechanisms of spontaneous curvature and softening in complex lipid bilayer mixtures

Henry J. Lessen, Kayla C. Sapp, Andrew H. Beaven, Rana Ashkar, and Alexander J. Sodt

Supplemental Material for "Molecular mechanisms of spontaneous curvature and softening in complex lipid bilayer mixtures"

Henry J. Lessen[1,*], Kayla C. Sapp[1,*], Andrew H. Beaven[1,2], Rana Ashkar[3,4], and Alexander J. Sodt[1,**]

[1]*Eunice Kennedy Shriver* National Institutes of Child Health and Human Development, National Institutes of Health, Bethesda, MD 20892
[2]Postdoctoral Research Associate Program, National Institute of General Medical Sciences, National Institutes of Health, Bethesda, MD 20892
[3]Department of Physics, Virginia Tech, Blacksburg, VA 24061
[4]Center for Soft Matter and Biological Physics, Virginia Tech, Blacksburg, VA 24061
[*]These two authors contributed equally.
[**]alexander.sodt@nih.gov

July 1, 2022

1 HMM state detection

A general overview of the HMM methodology used in this study will be provided. First, dimer conformations are extracted from MD trajectories from user defined parameters that will be described in detail below. These structures are clustered and subsequently divided into HMM observables that describe the energy landscape. The HMM observables are then used to define hidden states and optimize parameters that define the model. The states are then used in additional calculations to determine curvature preference of specific dimer subpopulations from their dynamic redistribution (curvature-coupled redistribution, CCR). A graphical summary of the steps in the HMM/CCR method is shown in Figure 1, and a list of terms is presented in Table S1.

Term	Meaning
Approach complex	A single instantaneous configuration of two lipids with centers separated by less than $R_{\text{pair}} = 14$ Å. A limited set of atoms of the approach complex are used to compute mean-squared-displacements (MSDs)
Similarity function	The criteria for judging the similarity of two approach complexes by weighting RMSD and hydrogen-bonding patterns. These are labeled as $\mathbf{S}$, with subscripts indicating function parameters.
Similarity center	A representative configuration from an ensemble of similar approach complexes. Determined by K-Medoid clustering [1]. The "center" of the cluster.
Similarity cluster	The set of approach complexes more similar to a particular similarity center than to any other similarity center. These are the observables of the HMM.
Pair trajectory	The time-ordered sequence of similarity cluster that is assigned to a pair of lipids.
HMM state	The target state of a lipid-lipid complex: A lipid pair possibly rich with structural and curvature-sensitive features, but which is identified only by the time sequence of its assigned similarity cluster. Determined by optimizing a HMM. The HMM state is computed by applying the HMM to a pair trajectory.
Hidden Markov model	The kinetic model of inter-conversion between hidden Markov states, and the probabilities of observing any HMM state as a member of a similarity cluster.

Table S1: Terms used to describe the configurations and models for developing the HMM.

1.1 Using an HMM to extract states

For example, PSM approach complexes are identified using five headgroup atoms from each PSM molecule (10 atom positions from each dimer). The atoms are { `OF`, `C1F`, `HNF`, `O3`, `HO3` }. For a complete list of atoms used to define approach complexes in each system analyzed, refer to Table S1. These atom positions are used to calculate the distance between molecules using the center of geometry. Pairs of lipids within $R_{\text{pair}} = 14$ Å were considered approach complexes. Atom positions are also used to calculate MSD between different approach complexes (used for scoring in K-medoid clustering).

We used approximately 15,000 approach complexes per simulation to define a pool from which the similarity centers were extracted. The set was extracted by traversing the trajectory uniformly, taking all complexes within R_{pair}. The quantity was limited by increasing the amount of trajectory skipped. Our software was able to efficiently determine similarity centers when the pool was less than 20,000.

Additional considerations must be made when identifying ion-mediated approach complexes. When processing simulations to extract this class of approach complex, an ion type and distance cutoff must be specified in the processing input file. When searching for the bridging ion, first the approach complex center (based on the specified atoms) is calculated. Then the distances from this point and the ions proximal to the approach complex are calculated to find the closest ion. If distance from the ion is then compared to the maximum radial distance (4 Å), this ion is taken as the bridging ion.

Construction of the HMM

K-medoid clustering [1] was used to reduce the complexity of the extracted approach complexes and identify HMM observable states. This method uses both the mean-square-displacement (MSD) between approach complexes (following rotational and translational alignment) and a heuristic hydrogen bond matching scheme to rank similarity between approach complexes. The unweighted MSD between two approach complexes with a matching hydrogen bond were reduced by ϵ_+ Å^2 for each bond, where ϵ_+ is a tunable parameter. If a hydrogen bond was present in one of the approach complexes but not the other, the MSD was penalized by ϵ_- Å^2. An exception was made for the amide-amide sphingolipid hydrogen bond. Penalties were applied that restricted members of a similarity cluster to have this bond (or the lack thereof) in common. The identity of one approach complex's **1** and **2** were swapped during the comparison, and the smaller MSD was selected, yielding a process independent of **1**/**2** ordering. The function applied by the K-medoid clustering to compare two pairs is called a similarity function, and any one function is denoted as $\mathbf{S}$, with $\epsilon_\pm$ parameters indicated in the subscript. The final value of the similarity function is denoted $\sim\chi^2$. For each similarity function, the number of medoid centers was set to 52, defining *similarity centers* labeled { A-Z, a-z }.

The data was then processed to describe the time evolution of the approach complexes using the similarity centers determined through K-medoid clustering.This is done by reiterating through the MD trajectory in order to assign individual approach complexes to specific similarity clusters throughout the simulation. When processing the MD trajectory to build the HMM, the same spacing used for extracting approach complexes was used. An approach complex was assigned the letter code of the medoid center with which it had the lowest $\sim\chi^2$. This yields many distinct series of similarity cluster observables, stored as simple character strings. These distinct series (called a pair trajectory) describe the evolution of independent approach complexes. The pair trajectories are then used to build the kinetic portion of the HMM.

Finally, we have to determine the "hidden" states used in our HMM, which will will refer to as HMM states. The model defines $N_s = 6$ states. There is no correct number of states no more than there is a correct model for any physical system. Rather, if "too many" states are selected, an interesting state may be split into two states that interchange rapidly, but which exchange slowly with the other states. If "too few" states are selected, features of interest can not sort cleanly into states. Quotes here indicate that these are qualitative judgments. Once states are determined, all approach complexes are then classified using the HMM states and used for further analysis, such as the curvature preference calculations described below.

2 PIP2: protonated on the 4- or 5-phosphate

Figure S2 shows the curvature coupling of PIP2 protonated on the 4-phosphate (left) and the 5-phosphate (right). While there are differences between the two states, results for each protonation state are consistent with the observation that PIP2-Ca^{2+}-POPC induces strong negative curvature.

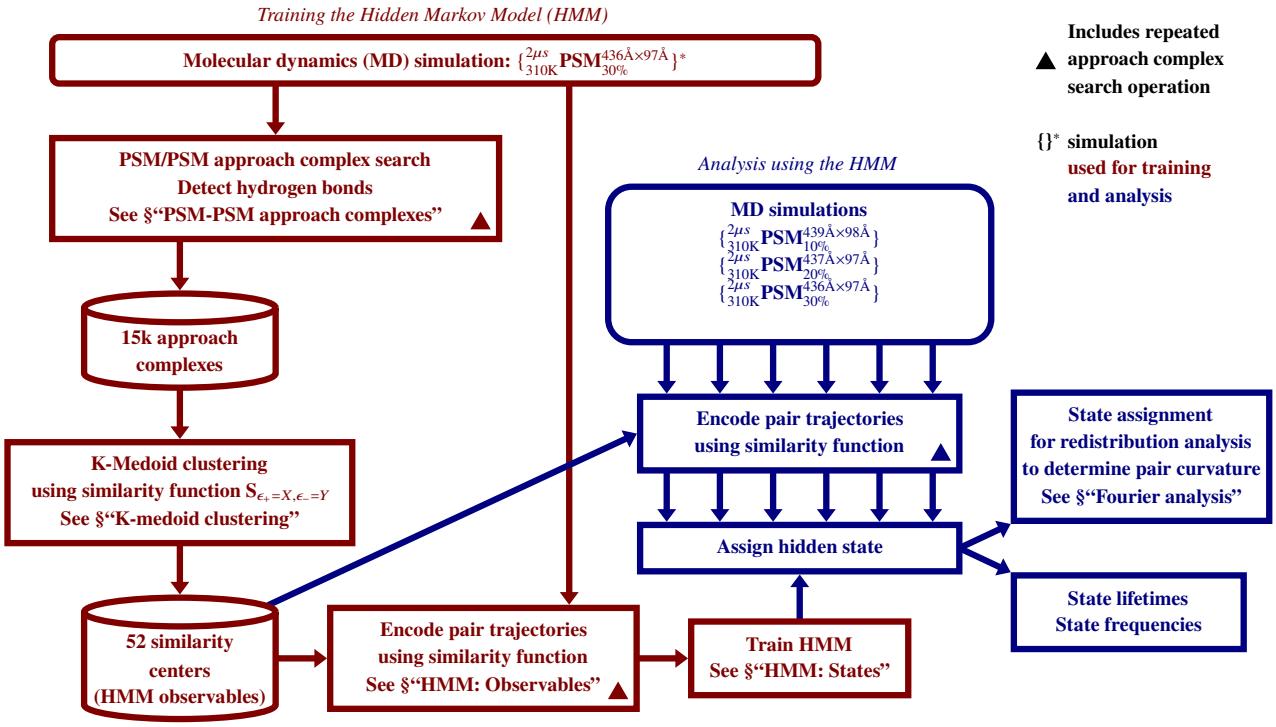

Figure S1: A flowchart showing the process of dimer discovery and assignment via a hidden Markov model (HMM). The training (left side) and analysis (right side) steps are distinguished by color.

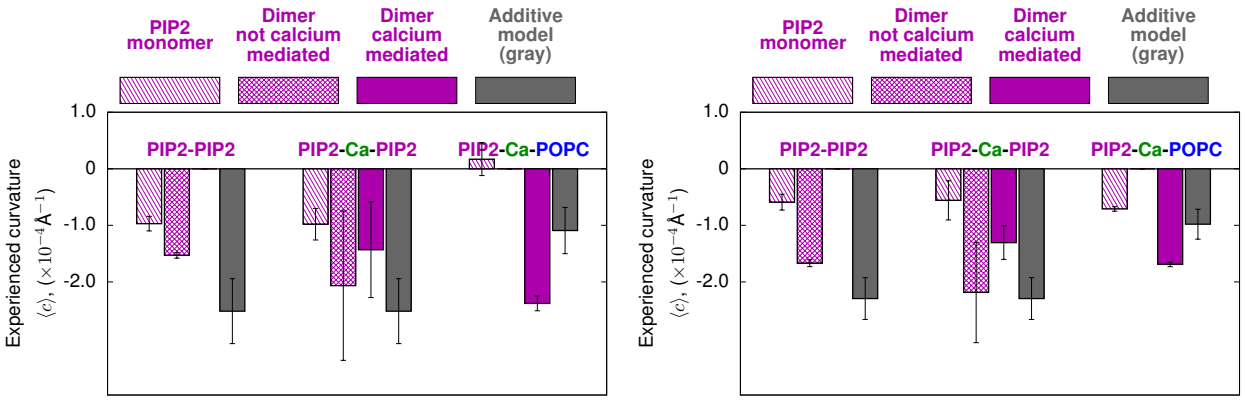

Figure S2: PIP2 protonated on the 4-phosphate (left) and the 5-phosphate (right).

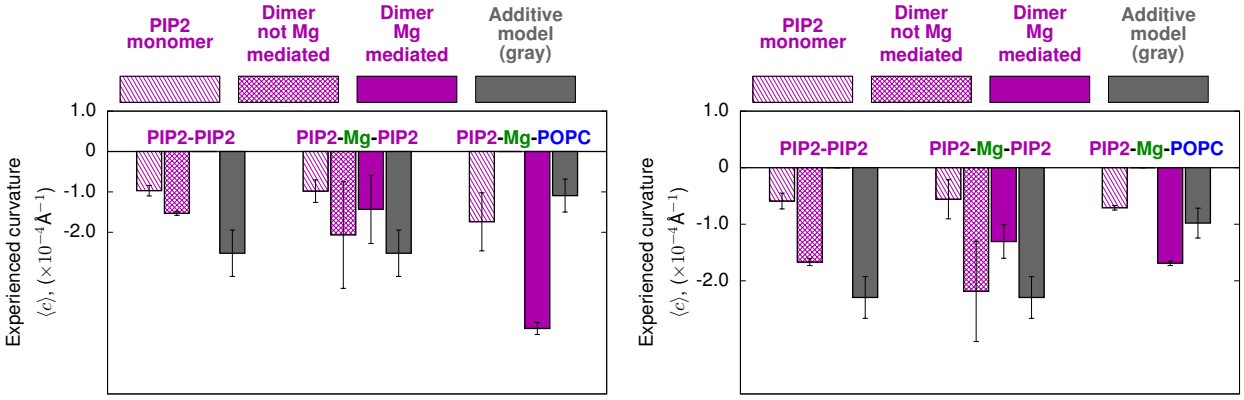

Figure S3: PIP2 spontaneous curvature, but now with interactions bridged by Mg^{2+}instead of Ca^{2+}. PIP2 is protonated either on the 4-phosphate (left) or the 5-phosphate (right).

State	P value	Pair Composition
Dimer (no HBond) to Dimer (HBond)	0.000077	
Dimer (no HBond) to Additive	0.025	DOPE to DOPE
Dimer (HBond) to Additive	0.21	
Dimer (no HBond) to Dimer (HBond)	0.0011	
Dimer (no HBond) to Additive	0.082	DOPE to DOPC
Dimer (HBond) to Additive	0.73	
Dimer (no HBond) to Dimer (HBond)	0.000083	
Dimer (no HBond) to Additive	0.0068	DOPE to DOPS
Dimer (HBond) to Additive	0.40	

Table S2: Results from Students T-test comparison of experienced curvatures determined from the DOPE/DOPC/DOPS simulations.

3 PIP2: Calcium vs. magnesium ions

Figure S3 shows the same curvature-dependent dimers now coupled by Mg^{2+}instead of Ca^{2+}. Results for $Mg^{2+}$are consistent with the mechanism that it is the cation-mediated interaction with neighboring generic phospholipid (here, POPC) that induces strong negative curvature.

State	P value	Pair Composition
Dimer to Additive	0.15	PIP2-PIP2
Dimer (No Calcium) to Dimer (Calcium)	0.15	
Dimer (No Calcium) to Additive	0.085	$PIP2 - Ca^{2+} - PIP2$
Dimer (Calcium) to Additive	0.040	
Monomer to Heterodimer	0.00039	$PIP2 - Ca^{2+} - POPC$
Heterodimer to Additive	0.0093	

Table S3: Results from Students T-test comparison of experienced curvatures determined from the PIP2/POPC simulations.

State	P value	Pair Composition
Dimer (no HBond) to Dimer (HBond)	0.19	
Dimer (no HBond) to Additive	0.094	10% PSM
Dimer (HBond) to Additive	0.75	
Dimer (no HBond) to Dimer (HBond)	0.070	
Dimer (no HBond) to Additive	0.021	20% PSM
Dimer (HBond) to Additive	0.71	
Dimer (no HBond) to Dimer (HBond)	0.0038	
Dimer (no HBond) to Additive	0.0029	30% PSM
Dimer (HBond) to Additive	0.061	

Table S4: Results from Students T-test comparison of experienced curvatures determined from the PSM simulations.

4 P values for comparisons of experienced curvatures

5 Softening theory for complex bilayers

With $c = c_1 + c_2$, where c_1 and c_2 are the two principal curvatures,

$$H_{\mathrm{HC}} = \frac{\kappa_{\mathrm{b}}}{2}(c_1 + c_2 - c_0)^2 + \bar{\kappa} c_1 c_2, \tag{S1}$$

the total elastic curvature energy is:

$$E_{\mathrm{HC}} = \frac{\kappa_{\mathrm{b}}}{2}\int_A \mathrm{d}\boldsymbol{S} H_{\mathrm{HC}}, \tag{S2}$$

To account for the preferred curvature $\Delta c_0 = c_{0,\mathrm{p}} - c_{0,\mathrm{background}}$ of a lipid ($c_{0,\mathrm{p}}$) in a background spontaneous curvature ($c_{0,\mathrm{background}}$), the energy density is modified by

$$H_{\mathrm{c}} = \frac{\kappa_{\mathrm{m}} A_p}{2}\int \mathrm{d}\boldsymbol{S}\big[\,(c - c_{0,\mathrm{p}})^2 - (c - c_{0,\mathrm{background}})^2\,\big], \tag{S3}$$

Here we do not include the Gaussian curvature modulus $\bar{\kappa}$ as we assume all lipids have equivalent $\bar{\kappa}$, and the integral of the Gaussian curvature does not vary with fluctuations.

For simplicity, the membrane surface, and thus its form in Eqs. S2 and S3, is parameterized in the linearized Monge gauge, a simplified surface parameterization capable of describing nearly planar configurations. The parameterization is $\boldsymbol{r}(x, y) = \{x, y, h(x, y)\}$ and linearization imposes a quadratic order cut-off [2, 3] that is accurate for thermal (here, weak) fluctuations:

$$E_{\mathrm{H}}\left[h(\boldsymbol{r})\right] = \int_A \mathrm{d}\boldsymbol{S}\,\frac{\kappa_{\mathrm{b}}}{2}\left[\boldsymbol{\nabla}^2 h(\boldsymbol{r})\right]^2 \tag{S4}$$

In Fourier space:

$$h(\boldsymbol{r}) = \frac{1}{A}\sum_{\boldsymbol{q}} h_{\boldsymbol{q}} \mathrm{e}^{\imath \boldsymbol{q}\cdot\boldsymbol{r}} \tag{S5}$$

$$h_{\boldsymbol{q}} = \int_A \mathrm{d}\boldsymbol{r} h(\boldsymbol{r}) \mathrm{e}^{-\imath \boldsymbol{q}\cdot\boldsymbol{r}}. \tag{S6}$$

For a real space function $f(\boldsymbol{r})$ the relation $f_{\boldsymbol{q}} = f^*_{-\boldsymbol{q}}$ applies to the Fourier transform coefficients. The coefficients are not independent. Furthermore, terms that must be real are real only if $\boldsymbol{q}$ and $-\boldsymbol{q}$ are considered simultaneously. In recognition of this we sum over $\boldsymbol{q}$ using the shorthand $\{\boldsymbol{q} > 0\}$,

$$\{\boldsymbol{q} > 0\} \equiv \{q_x, q_y\} \tag{S7}$$

such that

$$\begin{cases} 0 < q_x < q_{\max} & \text{for } q_y = 0 \\ -q_{\max} < q_x < q_{\max} & \text{for } q_y > 0 \end{cases},$$

yielding two independent functions, $f_{\boldsymbol{q},a}$ and $f_{\boldsymbol{q},b}$:

$$\begin{aligned} f_{\boldsymbol{q},a}(\boldsymbol{r}) &= 2\mathrm{Re}\, f_{\boldsymbol{q}} \cos(\boldsymbol{q}\cdot\boldsymbol{r}) \\ f_{\boldsymbol{q},b}(\boldsymbol{r}) &= 2\mathrm{Im}\, f_{\boldsymbol{q}} \sin(\boldsymbol{q}\cdot\boldsymbol{r}) \end{aligned} \tag{S8}$$

Henceforth we use the cos function's coefficient $f_{\boldsymbol{q},a} = 2\mathrm{Re}\, f_{\boldsymbol{q}}$ as the independent variable. Implicitly, the same derivations apply to the b-component, $h_{\boldsymbol{q},b}$.

The Fourier coefficients $\{\, h_{\boldsymbol{q},a} \,\}$ of the height (with $h_{\boldsymbol{q},b}$ defined analogously to $f_{\boldsymbol{q},b}$) are energetically uncoupled:

$$E_{\mathrm{H}}\left(\{h_{\boldsymbol{q},a}\}\right) = \frac{\kappa_{\mathrm{b}}}{2A} \sum_{\{\boldsymbol{q}>0\}} q^4 h_{\boldsymbol{q},a}^2 \tag{S9}$$

with all other cross-terms energetically uncoupled at this order. Given a bilayer with a mole fraction χ of one lipid and $1-\chi$ background lipids, the energy of a density fluctuation is given by

$$\begin{aligned} E_{\rho}\left(\{p_{\boldsymbol{q},a}\}\right) &= \sum_{\{\boldsymbol{q}>0\}} \frac{k_{\mathrm{B}}T(p_{\boldsymbol{q},a}^2)}{2A\rho_0\left(1-\chi\right)} \\ &= \sum_{\{\boldsymbol{q}>0\}} \frac{A_p k_{\mathrm{B}}T(p_{\boldsymbol{q},a}^2)}{4A\chi\left(1-\chi\right)} \end{aligned} \tag{S10}$$

Where $p_{\boldsymbol{q},a}$ are Fourier coefficients for the distribution of particles (with a and b subscripts analogous to $f_{\boldsymbol{q},a}/f_{\boldsymbol{q},b}$ above), and $\rho_0 = \frac{2\chi}{A_p}$, with the factor of two representing the contribution from each leaflet. See derivation below.

The impact of the distribution of lipids with spontaneous curvature difference $\Delta c_{0,\mathrm{p}}$ is now introduced using the lipid density $\rho(\boldsymbol{r})$ which is convoluted with the spatial extent $w(\boldsymbol{r})$ to account for the change in curvature energy density in Eq. S3:

$$\begin{aligned} E_{\mathrm{c}}\left[h(\boldsymbol{r}),\rho(\boldsymbol{r})\right] &= \frac{\kappa_{\mathrm{m}}}{2}\int_{L^2} \mathrm{d}\boldsymbol{r}_p \int_{L^2} \mathrm{d}\boldsymbol{r}\rho(\boldsymbol{r}_p) w(\boldsymbol{r}-\boldsymbol{r}_p)\times \\ &\quad \left[\left(\boldsymbol{\nabla}^2 h(\boldsymbol{r}) - c_{0,\mathrm{p}}\right)^2 - \left(\boldsymbol{\nabla}^2 h(\boldsymbol{r})\right)^2 - c_{0,\mathrm{background}}\right] \\ &= \frac{A_p\kappa_{\mathrm{m}}}{2}\int_{L^2} \mathrm{d}\boldsymbol{r}\rho(\boldsymbol{r})\times \\ &\quad \left[\left(\boldsymbol{\nabla}^2 h(\boldsymbol{r}) - c_{0,\mathrm{p}}\right)^2 - \left(\boldsymbol{\nabla}^2 h(\boldsymbol{r})\right)^2 - c_{0,\mathrm{background}}\right] \end{aligned} \tag{S11}$$

Here Eq. S12 uses $w(\boldsymbol{r}-\boldsymbol{r}_p) = A_p\delta(\boldsymbol{r}-\boldsymbol{r}_p)$ as justified by the observed locality of PC, PE, and PS [4].

Performing the Fourier transform of Eq. S11 yields the particle-distribution/undulation coupling:

$$E_{\mathrm{c}}\left(\{h_{\boldsymbol{q},a}\},\{p_{\boldsymbol{q},a}\}\right) = -\sum_{\{\boldsymbol{q}>0\}} \frac{A_p\Delta c_{0,\mathrm{p}}\kappa_{\mathrm{m}} q^2 p_{\boldsymbol{q},a} h_{\boldsymbol{q},a}}{A}. \tag{S12}$$

with $p_{\boldsymbol{q},a}$ the Fourier coefficient for the density of lipid with spontaneous curvature differ $\Delta c_{0,\mathrm{p}} = c_{0,\mathrm{p}} - c_{0,\mathrm{background}}$. Combining Eqs. S9, S10, and S12, the total energy is

$$E_a = E_{\mathrm{H}}\left(\{h_{\boldsymbol{q},a}\}\right) + E_{\rho}\left(\{p_{\boldsymbol{q},a}\}\right) + E_{\mathrm{c}}\left(\{h_{\boldsymbol{q},a}\},\{p_{\boldsymbol{q},a}\}\right). \tag{S13}$$

The expectation of $h_{\boldsymbol{q},a}^2$ is determined by

$$\langle h_{\boldsymbol{q},a}^2\rangle = Z^{-1}\int \mathrm{d}h_{\boldsymbol{q},a}\mathrm{d}p_{\boldsymbol{q},a} h_{\boldsymbol{q},a}^2 \mathrm{e}^{-\beta E_a}, \tag{S14}$$

where

$$Z = \int \mathrm{d}h_{\boldsymbol{q},a}\mathrm{d}p_{\boldsymbol{q},a}\mathrm{e}^{-\beta E_a}. \tag{S15}$$

For a single-component membrane ($\chi = 0$ or $\Delta c_{0,\mathrm{p}} = 0$), integration leads to

$$\langle h_{\boldsymbol{q},a}^2\rangle = \frac{A k_{\mathrm{B}}T}{\kappa_{\mathrm{b}} q^4} \quad \text{(single component)}, \tag{S16}$$

from which the bending rigidity can be determined. For the two-component mixture, the expectation of $h^2_{\boldsymbol{q},a}$ is now:

$$\langle h^2_{\boldsymbol{q},a}\rangle = \frac{Ak_{\mathrm{B}}T}{\kappa_{\mathrm{b}}q^4}(1+\frac{\Delta c^2_{0,\mathrm{p}}A_p\kappa_{\mathrm{b}}\chi\,(1-\chi)}{2k_{\mathrm{B}}T}+\mathcal{O}[\Delta c^3_{0,\mathrm{p}}]) \tag{S17}$$

Thus, a bilayer with a symmetric or asymmetric mixture of lipids (with unequal spontaneous curvatures) will experience apparent softening according to

$$\begin{aligned}\kappa_{\mathrm{apparent}} &= \kappa_{\mathrm{b}}\left(1-\frac{\Delta c^2_{0,\mathrm{p}}A_p\kappa_{\mathrm{b}}\chi\,(1-\chi)}{2k_{\mathrm{B}}T}\right)\\ &= \kappa_{\mathrm{b}}\,(1-\alpha)\,.\end{aligned} \tag{S18}$$

where α is the same as in Eq. 2 of the main text.

5.1 Fourier amplitudes of variations in lipid density

The derivation for the free-energy/entropic variation of the Fourier amplitudes of the density modes follows below.

Consider a bilayer with mol fraction χ of lipid A and $1-\chi$ of background lipids. Break the bilayer into M narrow strips that are long in y with length L_y and narrow in x with width d. There are N lipids in each strip. The expected number of lipid A, $\langle n_A\rangle$ in each narrow strip is χN. Given random fluctuations, the variance of n_A is $\chi(1-\chi)N$ according to the binomial distribution. For convenience define the density fluctuation function $\rho_A(i)$ as:

$$\Delta n_A(i) = n_A(i) - \chi N \tag{S19}$$

If the number of lipids in bin i, $n_A(i)$ is independent of $n_A(j)$, the autocorrelation function of $\Delta n_A(i)$, $r_{nn}(j-i)$ is

$$r_{nn}(j-i) = \begin{cases}\chi(1-\chi)N & : j=i\\ 0 & : j\neq i\end{cases} \tag{S20}$$

By the Wiener-Kninchin theorem, the power spectral density $S(f)$ is

$$\begin{aligned}S(f) &= \sum_{k=-\infty}^{\infty} r_{nn}(k)\mathrm{e}^{-i2\pi fk}\\ &= \chi(1-\chi)N,\end{aligned} \tag{S21}$$

that is, $S(f)$ is independent of f; it is "white noise." Given the power spectral density $S(f)$ in Eq. S21, discrete variables can be translated to the continuous case of interest: the Fourier transform of the lateral distribution of lipid A density, p_q. Dividing by the bin area dL_y, transforming from f to q with $f=\frac{qL_x}{2\pi}$, and multiplying by 2 π (by the convention in which the factor of $(2\pi)^{-1}$ is in the *inverse* transform) yields:

$$S(q) = (2\pi)\frac{L_x}{2\pi}\frac{1}{dL_y}S(f) \tag{S22}$$

$$= L_x\rho_A(1-\chi) \tag{S23}$$

Where here $\rho_A = \frac{N\chi}{dL_y}$ is the number of lipids per unit area. Instead of restricting analysis to x, performing the two-dimensional Fourier analysis with $\boldsymbol{q}=\{q_x,q_y\}$ yields

$$S(\boldsymbol{q}) = (1-\chi)A\rho_A \tag{S24}$$

Given a sufficiently large bilayer, we now substitute a normal distribution with matching variance. The probability $\mathrm{pr}(p_{\boldsymbol{q}})$ of observing density fluctuation $p_{\boldsymbol{q}}$ is given by

$$\mathrm{pr}(p_{\boldsymbol{q}}) \propto \exp(-\frac{p^2_{\boldsymbol{q},a}+p^2_{\boldsymbol{q},b}}{(1-\chi)A\rho_A}) \tag{S25}$$

where A_p is the area of the lipid, $p_{\boldsymbol{q},a}$ and $p_{\boldsymbol{q},b}$ are defined as for $h_{\boldsymbol{q},a}/h_{\boldsymbol{q},b}$ above. The expectation value $\langle p^2_{\boldsymbol{q}}\rangle$:

$$\langle|p_{\boldsymbol{q}}|^2\rangle = Z^{-1}\int_{-\infty}^{\infty}\int_{-\infty}^{\infty}\mathrm{d}p_{\boldsymbol{q},a}\mathrm{d}p_{\boldsymbol{q},b}(p^2_{\boldsymbol{q},a}+p^2_{\boldsymbol{q},b})\mathrm{e}^{-\frac{p^2_{\boldsymbol{q},a}+p^2_{\boldsymbol{q},b}}{(1-\chi)A\rho_A}} \tag{S26}$$

$$= (1-\chi)A\rho_A \tag{S27}$$

with

$$Z = \int_{-\infty}^{\infty} \int_{-\infty}^{\infty} \mathrm{d}p_{\boldsymbol{q},a} \mathrm{d}p_{\boldsymbol{q},b} \mathrm{e}^{-\frac{p_{\boldsymbol{q},a}^2 + p_{\boldsymbol{q},b}^2}{(1-\chi)A\rho_A}} \tag{S28}$$

has yielded the correct variance.

6 Tabulated simulation details

System/composition	Ions	Dimensions	Duration
30% DOPE, 25% DOPC, 45% DOPS	125 Cl^- 697 Na^+	429×95×86 Å^3	4 × 600 ns
10% PIP2 (half protonated on P_4, half on P_5) 90% POPC	82 Cl^- 129 Ca^{2+}	125×125×84 $Å^3$	1×2 μs
10% PIP2 (half protonated on P_4, half on P_5) 90% POPC	82 Mg^{2+} 129 Ca^{2+}	125×125×84 $Å^3$	1×2 μs
10% PSM 90% POPC	none	432×98×95 Å^3	1×1.1 μs
20% PSM 80% POPC	none	423×98×97 Å^3	1×1.1 μs
30% PSM 70% POPC	none	415×98×98 Å^3	1×1.1 μs

Table S5: Key descriptors of the simulations analyzed in this work.

References

[1] Kaufman L. and Rousseeuw P. Clustering by means of Medoids. In *Statistical Data Analysis Based on the L1 Norm and Related Methods*, pages 405–416, 1987.

[2] Frank L.H. Brown. Elastic modeling of biomembranes and lipid bilayers. *Annual Review of Physical Chemistry*, 59:685–712, 2008.

[3] Markus Deserno. Fluid lipid membranes: From differential geometry to curvature stresses. *Chemistry and Physics of Lipids*, 185:11–45, 2015.

[4] Kayla C. Sapp, Andrew H. Beaven, and Alexander J. Sodt. Spatial extent of a single lipid's influence on bilayer mechanics. *Physical Review E*, 103(4), 2021.